We are IntechOpen, the world's leading publisher of Open Access books Built by scientists, for scientists

4,800
Open access books available

122,000
International authors and editors

135M
Downloads

Our authors are among the

154
Countries delivered to

TOP 1%
most cited scientists

12.2%
Contributors from top 500 universities

CLARIVATE ANALYTICS BOOK CITATION INDEX INDEXED

WEB OF SCIENCE™

Selection of our books indexed in the Book Citation Index in Web of Science™ Core Collection (BKCI)

Interested in publishing with us?
Contact book.department@intechopen.com

Numbers displayed above are based on latest data collected.
For more information visit www.intechopen.com

Chapter 1

Development of a Coupled Fluid-Structure Model with Application to a Fishing Net in Current

Chunwei Bi, Yunpeng Zhao and Guohai Dong

Additional information is available at the end of the chapter

http://dx.doi.org/10.5772/58931

1. Introduction

Aquaculture is expanding all over the world, and the net cage is becoming prevalent in the aquaculture industry. Good knowledge of the hydrodynamic characteristics of the net cage has important significance to the design of the net cage and the welfare of the fish. An important component of a net cage is the fishing net, where the fish are kept and grown. The fishing net is completely submerged and infinitely flexible. When exposed to current, the fishing net changes its shape to reduce the hydrodynamic force acting on it, and the deformed net in turn affects the flow field around the fishing net. In this way, the flow field and the deformation of the fishing net interact and mutually influence each other. Therefore, it is very necessary to consider the fluid-structure interaction between flow and the fishing net when calculating the hydrodynamic characteristics of the net cage.

To investigate the hydrodynamic characteristics of net cages, much progress has been made by both experimental measurements and numerical simulations. Aarsnes et al. [1] conducted a series of physical model tests to measure the flow-velocity reduction, fishing-net deformation and the drag force acting on net cages. Lader and Enerhaug [2] performed experiments to investigate the forces and geometry of a net cage in uniform flow, and the flow-velocity reduction in the centre of the net cage was given as 20%. It was found that the global forces acting on a flexible fishing net were not proportional to the square of the flow velocity for all currents. Fredriksson et al. [3] conducted a numerical study on mooring tensions of a large fish farm containing 20 net cages while the flow-velocity reduction was estimated using a simplified control volume approach. DeCew et al. [4] investigated the submergence behavior of a fish cage in a single-point mooring system under currents by a numerical model and a reduction of 12.7% of the current velocity was applied to the aft portion of the net chamber. Huang et al. [5] and Xu et al. [6] analyzed the hydrodynamic behaviors of net cages in waves

and a reduction factor of 0.85 was adopted in the numerical model to represent the retardation effect on the water particle speed after passing through each previous net.

Based on the above analysis, the reduction in current downstream from the fishing net has been taken into consideration in studying the hydrodynamic force and the effective volume of the net cage. However, only a reduction factor was estimated to represent the shielding effect of the fishing net for most of the numerical works. There has not been a numerical model focusing on the fluid-structure interaction between flow and a flexible net. As an extension of our previous works [7-8], a coupled fluid-structure model is developed based on a joint use of the porous-media fluid model and the lumped-mass mechanical model. Using an appropriate iterative scheme, the fluid-structure interaction between flow and fishing net can be solved.

2. Model descriptions

The coupled model includes two numerical models: the porous-media fluid model and the lumped-mass mechanical model. The porous-media fluid model can simulate the flow field around a plane net with no deformation, and the lumped-mass mechanical model can simulate the deformation of fishing net in certain current. The joint use of the above two models is presented to solve the fluid-net interaction problem in current. The steady flow field around fishing net can be obtained by using an appropriate iterative scheme as explained later in Section 2.3. This model has been introduced detailed in our previous studies [9-10].

2.1. The porous-media fluid model

The flow field around a plane net is simulated using a commercial computational fluid dynamics (CFD) software FLUENT from ANSYS Inc. The porous-media fluid model is introduced to model the plane net, and the finite volume method is used to solve the governing equations of the numerical model. Thus, a brief review of the porous-media fluid model is given here.

The governing equations of the porous-media fluid model are mainly the Navier-Stokes equations as follows:

$$\frac{\partial \rho}{\partial t} + \frac{\partial \left(\rho u_i \right)}{\partial x_i} = 0 \tag{1}$$

$$\frac{\partial \left(\rho u_i \right)}{\partial t} + \frac{\partial \left(\rho u_i u_j \right)}{\partial x_j} = -\frac{\partial P}{\partial x_i} + \rho g_i + \frac{\partial}{\partial x_j}\left(\mu + \mu_t \right)\left(\frac{\partial u_i}{\partial x_j} + \frac{\partial u_j}{\partial x_i} \right) + S_i \tag{2}$$

where t is time; μ and ρ are the viscosity and the density of the fluid, respectively; μ_t is the eddy viscosity; $P=p+(2/3)\rho k$, where p is pressure; k is the turbulent kinetic energy; u_i and u_j are

http://dx.doi.org/10.5772/58931

the average velocity components, respectively; g_i is the acceleration due to gravity; i, j=1, 2, 3 (x, y, z); and S_i is the source term for the momentum equation.

The porous-media fluid model is a hypothetical model which produces the same water-blocking effect as the fish net by setting the coefficients of the hypothetical porous media. For flow through porous media, a pressure gradient exists:

$$\nabla p = \mathrm{a}\vec{u} + \mathrm{b}\left|\vec{u}\right|\vec{u} \tag{3}$$

where a and b are constant coefficients and $\vec{u}$ is the flow velocity. This expression was proposed by Forchheimer in 1901 based on the Darcy law. For large porosity (e.g., an array of fixed cylinders), turbulence will occur and the quadratic term for the frictional force will completely dominate over the viscous term (the linear term) [11]. In this case, the linear term is only a fitting term which has no physical meaning and thus it can be neglected.

Outside the porous media, the source term for the momentum equation is given by S_i=0. Inside the porous media, S_i is calculated by the following equation:

$$S_i = -C_{ij}\frac{1}{2}\rho\left|\vec{u}\right|\vec{u} \tag{4}$$

where C_{ij} is given by

$$C_{ij} = \begin{pmatrix} C_n & 0 & 0 \\ 0 & C_t & 0 \\ 0 & 0 & C_t \end{pmatrix} \tag{5}$$

where C_{ij} represents material matrices consisting of porous media resistance coefficients, C_n is the normal resistance coefficient, and C_t is the tangential resistance coefficient.

For flow through the porous media, the drag force (F_d) and the lift force (F_l) acting on it can be expressed as follows:

$$\overrightarrow{F_d} = C_n\frac{1}{2}\rho\lambda A\left|\vec{u}\right|\vec{u} \tag{6}$$

$$\overrightarrow{F_l} = C_t\frac{1}{2}\rho\lambda A\left|\vec{u}\right|\vec{u} \tag{7}$$

where λ is the thickness of the porous media and A is the area of the porous media.

The porous coefficients in Eqs. (6) and (7) can be calculated from the drag and lift forces, while the drag and lift forces acting on a fishing net have strong relationship with the features of the net. So the connection between net features and flow field is built by the porous coefficients in the numerical model. Generally, the drag and lift forces of the plane net are obtained from laboratory experiments. These forces can also be calculated from the Morison equation:

$$F_d = \frac{1}{2}\rho C_d A u^2 \tag{8}$$

$$F_l = \frac{1}{2}\rho C_l A u^2 \tag{9}$$

where C_d and C_l are coefficients that can be calculated using empirical formulas [1, 12-14].

The porous coefficient C_n can be calculated from a curve fit between drag forces acting on a plane net and corresponding current velocities using the least squares method when the plane net is oriented normal to the flow. The other coefficient C_t can be obtained when a plane net is oriented at an attack angle (see Figure 1a). In this case, the coefficient C_t should be transformed into $C_{t\alpha}$ using Eq. (10) [15]. Next, $C_{t\alpha}$ can be calculated from a curve fit between lift forces acting on a plane net and corresponding current velocities using the least squares method.

$$C_{t\alpha} = \frac{C_n - C_t}{2}\sin(2\alpha) \tag{10}$$

where α is the attack angle that is defined to be the angle between the flow direction and the plane net in the horizontal plane; $C_{t\alpha}$ is the tangential inertial resistance coefficient for the plane net at an attack angle α.

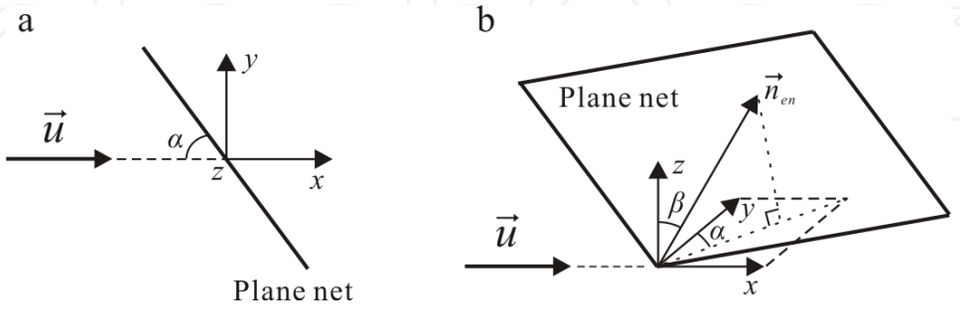

Figure 1. Definition of the angles α and β: (a) a plane net in the horizontal plane and (b) a plane net at an arbitrary position.

When a plane net is oriented at an arbitrary position (see Figure 1b), the porous coefficients should be transformed using Eq. (11):

$$\begin{pmatrix} C_n' \\ C_t' \\ C_t' \end{pmatrix} = \begin{pmatrix} \sin^2\alpha\sin^2\beta & \cos^2\alpha & \sin^2\alpha\cos^2\beta \\ \frac{1}{2}\sin 2\alpha\sin^2\beta & -\frac{1}{2}\sin 2\alpha & \frac{1}{2}\sin 2\alpha\cos^2\beta \\ \frac{1}{2}\sin 2\beta & 0 & -\frac{1}{2}\sin 2\beta \end{pmatrix} \begin{pmatrix} C_n \\ C_t \\ C_t \end{pmatrix} \tag{11}$$

where β is the angle between the normal vector of the plane net ($\vec{n}_{en}$) and the z-direction. It should be noted that the cosines of α and β can be calculated between the corresponding two vectors.

2.2. The lumped-mass mechanical model

The lumped-mass mechanical model is introduced to simplify the fishing net, and the motion equations can be established mainly based on Newton's Second Law. Given an initial net configuration, the motion equations can be solved numerically for each lumped-mass point. Finally, the configuration of the net in current can be simulated. The calculation method for the model has been explained fully in our previous studies [16-17]. Here only a brief outline is described.

In a uniform current, the motion equations of lumped-mass point i can be expressed as follows:

$$(M_i + \Delta M_i)\vec{a} = \sum_{j=1}^{n} \vec{T}_{ij} + \vec{F}_d + \vec{B} + \vec{W} \tag{12}$$

where M_i and ΔM_i are the mass and added mass of lumped-mass point i, $\vec{a}$ is the acceleration of the point, $\vec{T}_{ij}$ is the tension force in twine ij (j is the code for the knot at another end of the bar ij), n is the number of adjacent knots of point i, $\vec{F}_d$, $\vec{W}$ and $\vec{B}$ are the drag force, gravity force and buoyancy force, respectively.

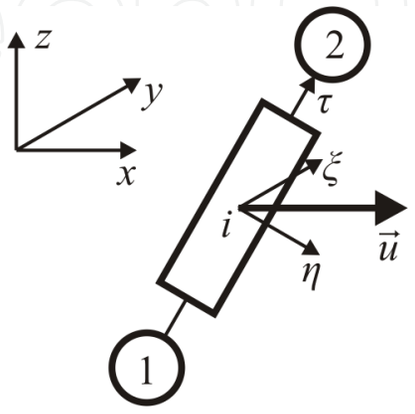

Figure 2. The local coordinate for a mesh twine.

To consider the direction of the hydrodynamic forces acting on mesh bars, local coordinates (τ, η, ξ) are defined to simplify the procedure (see Figure 2). The origin of the local coordinate is set at the center of a mesh bar, and the η-axis lies on the plane including τ-axis and flow velocity $\vec{u}$. The drag force on a lumped-mass point in the τ-direction can be obtained from the Morison equation as follows:

$$F_{D\tau} = -\frac{1}{2}\rho C_{D\tau} A_{\tau} \left|\vec{V}_{\tau} - \vec{\dot{R}}_{\tau}\right| (\vec{V}_{\tau} - \vec{\dot{R}}_{\tau}) \tag{13}$$

where $C_{D\tau}$ is the drag coefficient in the τ-direction, A_{τ} is the projected area of the twine normal to the τ-direction, $\vec{\dot{R}}_{\tau}$ and $\vec{V}_{\tau}$ are the velocity components of the lumped-mass point and water particle in the τ-direction. Similar expressions can be applied to the other two components of the drag force: $F_{D\eta}$ and $F_{D\xi}$.

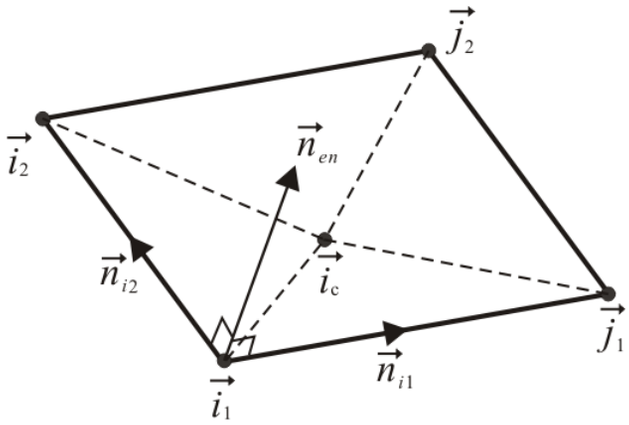

Figure 3. Schematic diagram of a plane-net element.

The mesh-grouping method [18-19] is used to reduce the computational effort of the net. Each grouped mesh is defined as a plane-net element (see Figure 3). The normal vector of the plane-net element ($\vec{n}_{en}$) is calculated as follows:

$$\vec{n}_{\text{en}} = \frac{\vec{n}_{i1} \times \vec{n}_{i2}}{\left|\vec{n}_{i1} \times \vec{n}_{i2}\right|} \tag{14}$$

where $\vec{n}_{i1}$ and $\vec{n}_{i2}$ are given by:

$$\vec{n}_{i1} = \frac{\vec{j}_1 - \vec{i}_1}{\left|\vec{j}_1 - \vec{i}_1\right|}, \vec{n}_{i2} = \frac{\vec{i}_2 - \vec{i}_1}{\left|\vec{i}_2 - \vec{i}_1\right|} \tag{15}$$

Because of the deformation of the net, the area of a plane-net element is not constant, thus impacting the solidity of the plane-net element. Consequently, the solidity S_n must be corrected accordingly based on the varying area of the plane-net element:

$$S_n^{'} = \frac{A}{A^{'}} S_n \tag{16}$$

where S_n and A are the solidity and area of the undeformed plane-net element, and $S_n^{'}$ and $A^{'}$ are the corrected solidity and area of the plane-net element. To calculate the area of the plane-net element, the four-sided element is divided into four triangles as shown in Figure 3. The area of the element can be obtained by the sum of the four triangles.

2.3. The coupled fluid-structure interaction model

Based on the above work, the interaction between flow and fishing net can be simulated by dividing the net into many plane-net elements (see Figure 4). The main concept of the numerical approach is to combine the porous-media fluid model and the lumped-mass mechanical model to simulate the interaction between flow and flexible nets. Taking a single flexible net as example, a calculating flow chart for the numerical approach is shown in Figure 5. A more detailed calculation procedure is given as follows.

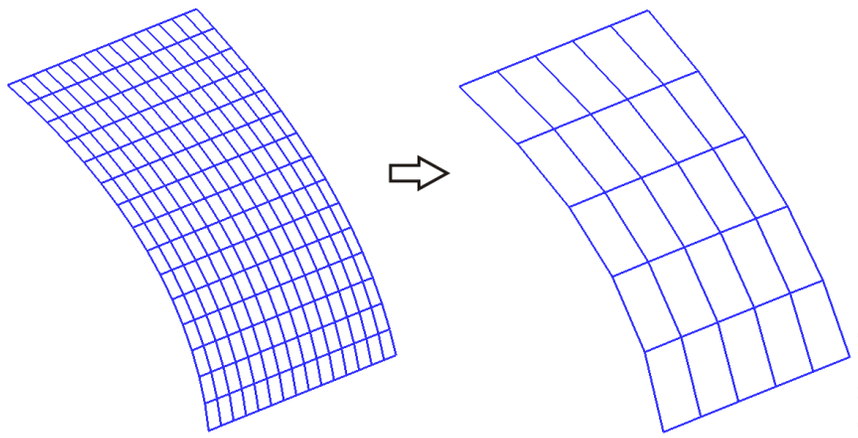

Figure 4. Schematic diagram of the net model.

The calculation procedure includes four steps. Step 1 is to simulate the flow field around a vertical plane net without considering the net deformation using the porous-media fluid model. Step 2 is to calculate the drag force and the configuration of a flexible net in current using the lumped-mass mechanical model. The given initial flow velocity is the average value exported from the upstream surface of the plane net in last step. In Step 3, according to the configuration of the net, the orientation and the porous coefficients of each plane-net element can be obtained, thus obtaining the flow field around the fishing net. In Step 4, the drag force

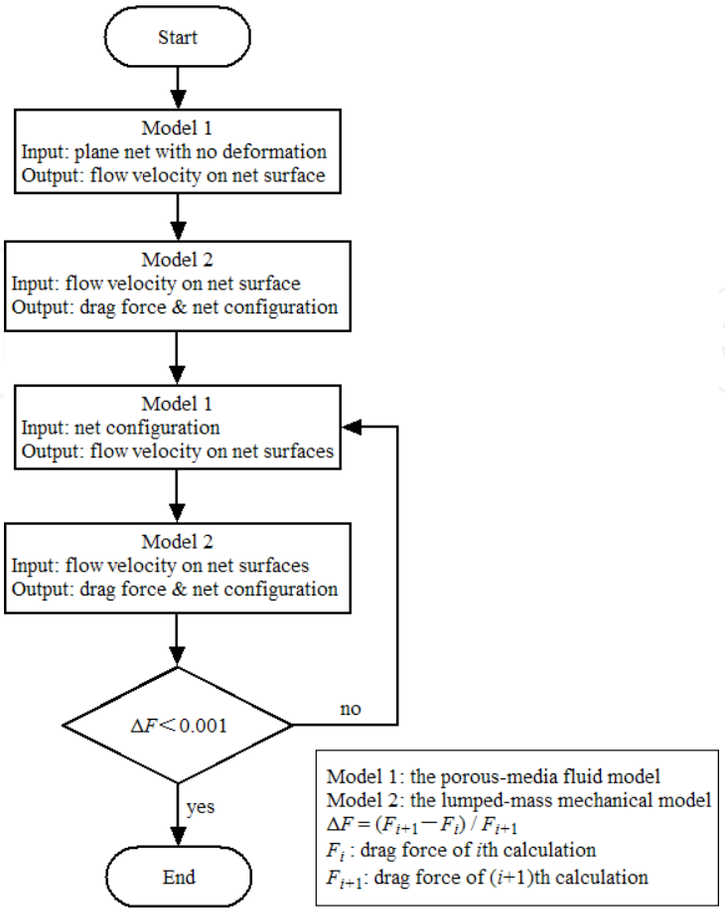

Figure 5. Flow chart of the coupled fluid-structure interaction model.

and the configuration of the net are calculated again. The flow velocity acting on each lumped-mass point is the average value exported from the upstream surface of the corresponding plane-net element in last step.

The terminal criterion of the calculation procedure is defined as $\Delta F = (F_{i+1} - F_i) / F_{i+1}$, where F_i and F_{i+1} are the drag forces of two adjacent calculations. If $\Delta F < 0.001$, it was determined that the force acting on the fishing net is stable and the configuration of the net is the equilibrium position considering the fluid-structure interaction. Thus the calculation procedure is completed. Otherwise, continue with the next iteration of the procedure and repeat Steps 3 and 4 until the criterion meets the precision requirement. Finally, the fluid-structure interaction problem can be solved and the steady flow field around the fishing net can be obtained.

3. Discussions of model parameters

Due to uncertainties in numerical simulation, convergence studies were performed to analyze the influence of different model parameters, such as thickness of the porous media, grid refinement, time-step size, number of net elements, number of iterations, porous coefficients,

etc. When varying one parameter, all other parameters were kept at their initial values as shown in Table 1.

Parameter	Value
Thickness of porous media	20 mm
Grid refinement	Grid 2 [a]
Time-step size	0.04 s
Number of net elements	5×5
Number of iterations	2
Porous coefficients	C_n=35.3 m^{-1}
	C_t=10.0 m^{-1}

Table 1. Initial values of the numerical model. [a] Main properties of the medium grid are shown in Table 2.

Grid	Min. cell size (mm)	Max. cell size (mm)	Total cells
Grid 1	5	50	413,697
Grid 2	10	50	117,294
Grid 3	20	50	49,807
Grid 4	10	60	34,492
Grid 5	10	70	21,124

Table 2. Main properties of the meshes used in the grid-refinement study.

The modeled net was a 0.3 m×0.3 m knotless polyethylene (PE) net with 15 meshes in width and 15 meshes in height. The twine diameter was 2.6 mm, and the mesh bar length was 20 mm. Mounted as square meshes, the net solidity ratio was 0.243.

3.1. Thickness of the porous media

A study on the thickness of the porous media was performed for a plane net at an attack angle α=90° and incoming velocity u_0=0.226 m/s. The corresponding Reynolds number is 5.88×10^2 calculated according to the twine diameter of the net. The dimensions of the porous media are the same as that of the fishing net in both width and height, and the porous media has a certain thickness. In order to investigate the influence of the thickness on the numerical results, the porous-media fluid model with different thicknesses, λ=5, 10, 20, 30, 40 and 50 mm, were performed.

The thickness of the porous media can affect the distribution of the flow velocity around the fishing net to some extent (see Figure 6). However, the numerical results of the flow velocity are almost the same for the thickness of 5, 10 and 20 mm. It was determined that the thickness

of the porous media does not affect the numerical results obviously until the thickness is greater than 20 mm. Therefore, a thickness of 20 mm is adopted hereafter for all the computations considering the total number of cells and computational accuracy. An increase in the thickness of the porous media can effectively reduce the number of cells, thus reducing the computational effort greatly. However, it is suggested that the maximum thickness of the porous media should not be greater than 10% of width or height of the plane net.

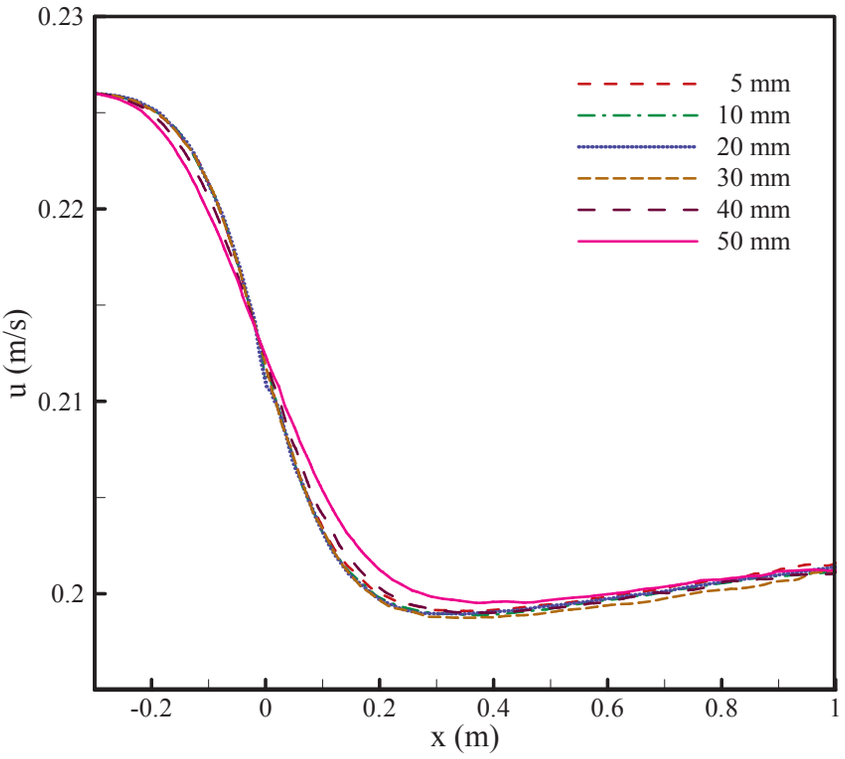

Figure 6. Numerical results of flow velocity *u* along the centerline of a plane net at different thickness of the porous media.

3.2. Grid refinement

The influence of grid on the numerical results was investigated by repeating the computations with different levels of refinement. Five grids as shown in Table 2 were taken into account. The minimum cell size was adopted inside the porous-media region. A growth rate of 1.2 was set around the net model, and the maximum cell size in the computational domain was set to control the distribution of the grid.

Numerical results of flow velocity obtained with different grids were compared (see Figure 7). It is found that numerical results are free of grid influence for Grid 1 and Grid 2. But for the coarser grid models, the numerical results tend to divergence, especially downstream from the fishing net. Therefore, Grid 2 is adopted hereafter for all the computations.

http://dx.doi.org/10.5772/58931

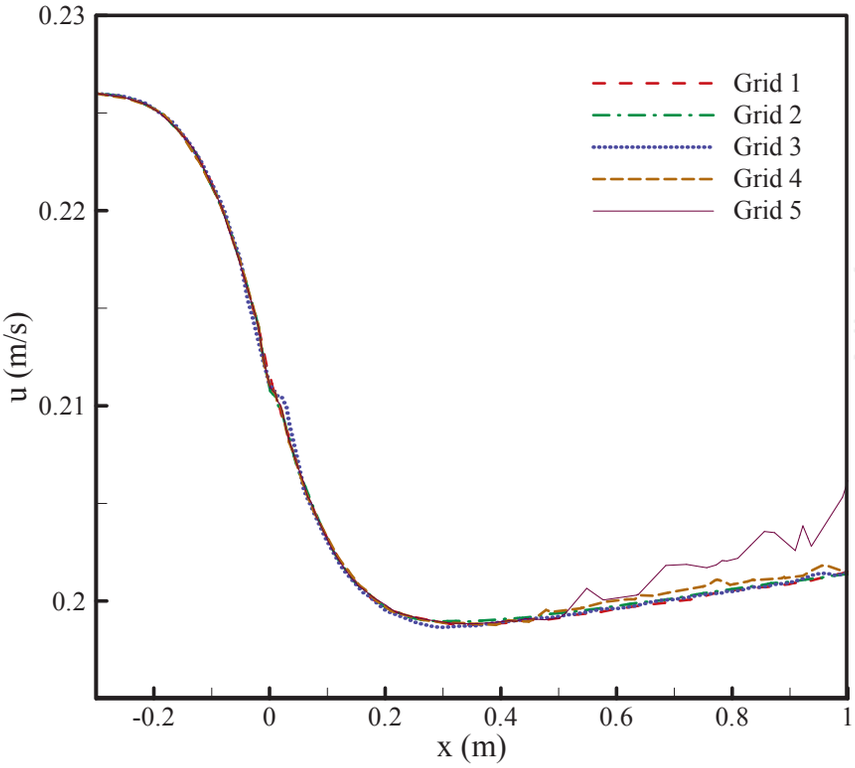

Figure 7. Numerical results of flow velocity *u* along the centerline of a plane net at different grids.

3.3. Time-step size

In order to investigate the influence of the time-step size, the computations were repeated with different time-step sizes: 0.01, 0.02, 0.04, 0.06, 0.08 and 0.10 s. The flow velocity both upstream and downstream from the plane net shows a convergence result for the time-step size smaller than 0.04 s (see Figure 8). Therefore, a time-step size of 0.04 s is adopted for computational effort saving. The computational effort decreases with increasing time-step size. However, it is suggested that the time-step size should not exceed the ratio between the minimum value of the cell size and the incoming velocity. Because the larger the time-step size is, the greater the residual error of each step will be, thus causing a divergence result without meeting the convergence criteria.

3.4. Number of plane-net elements

In the numerical model, each mesh is defined as a plane-net element. In order to reduce the computational effort, the mesh-grouping method was used to reduce the number of plane-net elements. The original model of the fishing net was a 15×15 model with 15 meshes in width and 15 meshes in height. Two grouped models were used to simplify the original model. For the original model, nine meshes were grouped into one mesh, thus obtaining a 5×5 model with a total of 25 elements. A 3×3 model with 9 elements can be obtained by grouping 25 meshes into one mesh.

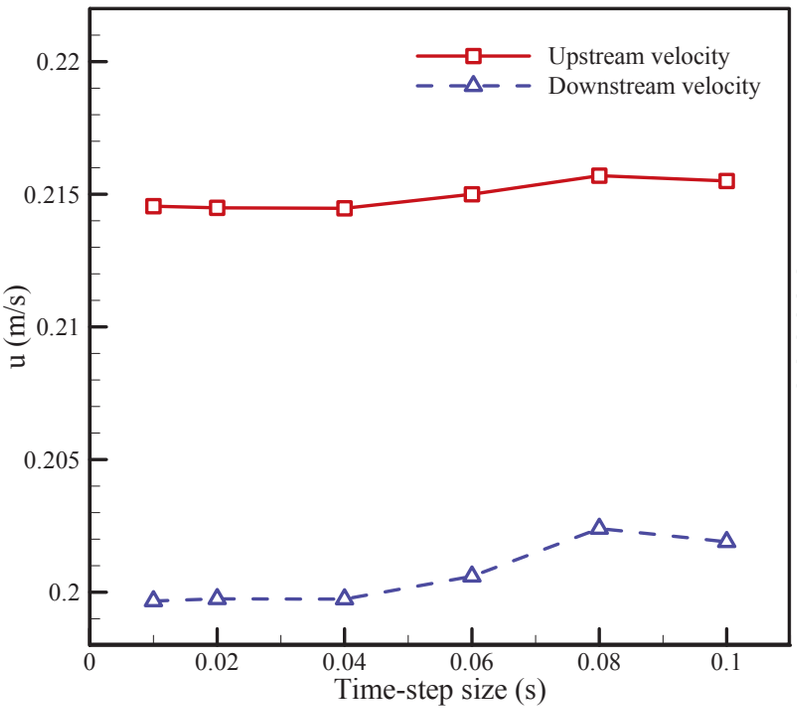

Figure 8. Numerical results of flow velocity *u* calculated with different time-step sizes. Upstream velocity is the average value exported from the upstream surface of the plane net. Downstream velocity is the flow velocity 0.6 m downstream from the center of the plane net, approximately twice the width of the plane net.

The calculated net configuration of the 5×5 model is almost coincided with that of the original 15×15 model (see Figure 9). The result of the 3×3 model agrees well with that of the original model except for a slight discrepancy at the bottom of the net. There is no significant difference between the results of flow velocity obtained with the grouped models and the original model (see Figure 10). Therefore, the mesh-grouping method can be used to reduce the number of plane-net elements without affecting the calculation accuracy. Because of better agreement on net configuration, the 5×5 model is chosen for further numerical simulations.

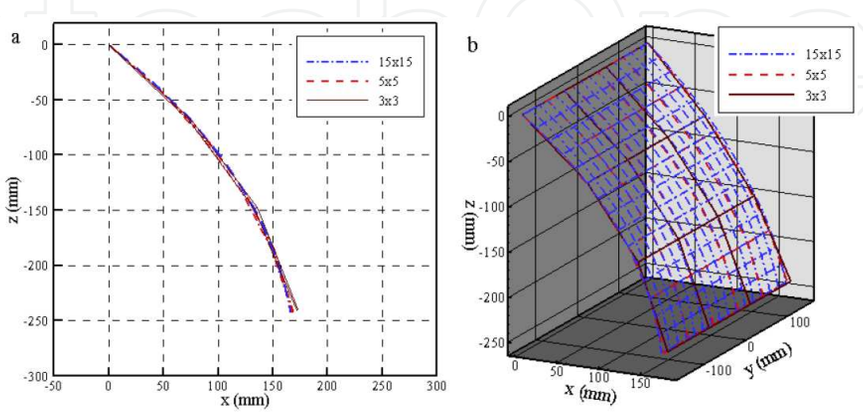

Figure 9. Comparison of the net configurations with different models for incoming velocity of 0.226 m/s: (a) side view and (b) 3D view.

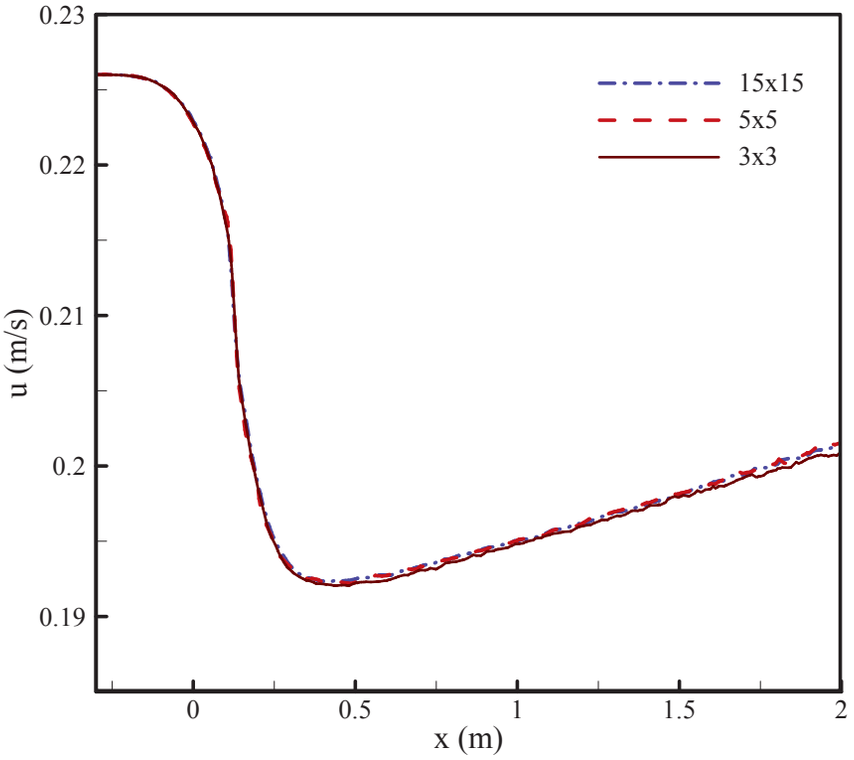

Figure 10. Comparisons of the flow-velocity component *u* along a line through the net in the *x*-direction obtained with different models for incoming velocity of 0.226 m/s. The straight line is *y*=0 on the horizontal plane *z*=–0.15 m.

3.5. Number of iterations

The interaction between flow and fishing net can be solved after several iterations. Taking a single net as example, the calculation precision reached the terminal criterion, $\Delta F < 0.001$, within two iterations, and the calculation procedure terminated for incoming velocity of 0.226 m/s. The drag-force difference between the 1st iteration and the 2nd iteration was approximately 0.7%. One more iteration was also calculated, and the result tended to converge.

Comparing the net configurations after different iterations, there is a little discrepancy between the 1st iteration and the 2nd iteration. However, the calculated net configuration of the 3rd iteration is almost coincided with that of the 2nd iteration (see Figure 11). The flow velocity upstream of the flexible net is greater than that of the plane net with no deformation, while the flow velocity downstream from the flexible net is smaller (see Figure 12). It was determined that the deformed net has more obvious shielding effect than the plane net with no deformation. There exists rather obvious discrepancy of the flow-velocity distribution between the 1st iteration and the 2nd iteration (see Figure 12), and the maximum discrepancy is approximately 6.3%. The result of the 2nd iteration is almost the same as that of the 3rd iteration, and the maximum discrepancy is approximately 0.17%. Therefore, two iterations is adopted to model a single net for computational effort saving.

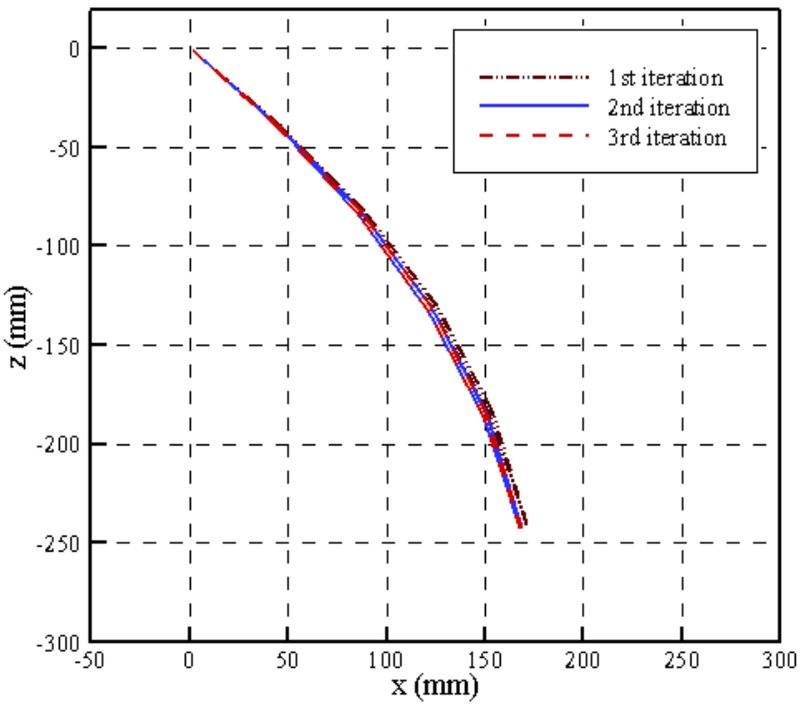

Figure 11. Comparison of the net configurations after different iterations for incoming velocity of 0.226 m/s.

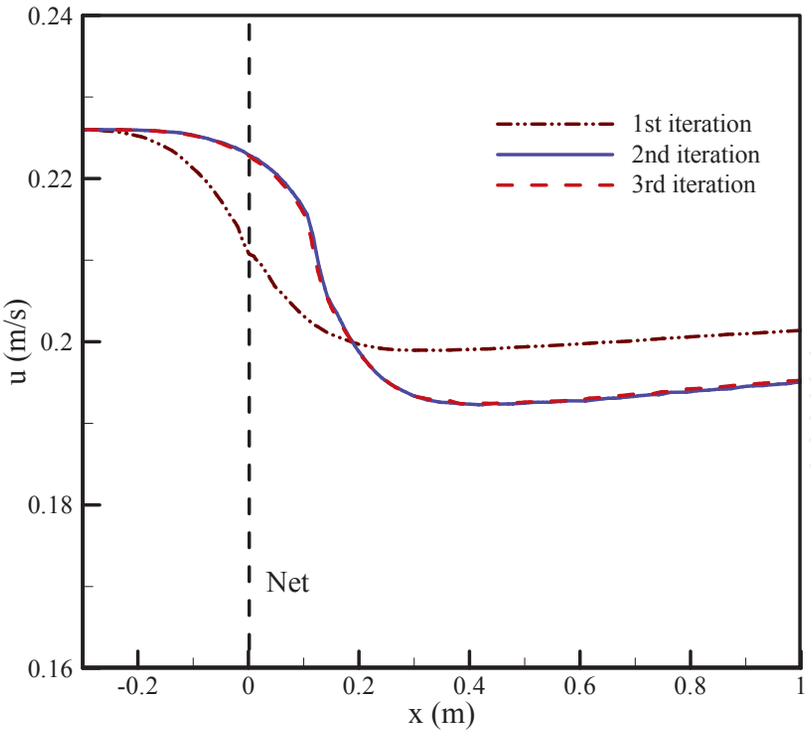

Figure 12. Comparisons of the flow-velocity component *u* along a line through the net in the *x*-direction after different iterations for incoming velocity of 0.226 m/s. The straight line is *y*=0 on the horizontal plane *z*=–0.15 m.

3.6. Porous coefficients

A set of porous coefficients, C_n=35.3 m^{-1} and C_t=10.0 m^{-1}, can be obtained from the experimental data (see Tables 3 and 4). The corresponding laboratory experiment is presented in our previous study [9]. Porous coefficients are key to the numerical results. Before the numerical simulations, a sensitivity study on the flow field with respect to the porous coefficients was carried out with a plane net at different attack angles.

u (m/s)	0.058	0.113	0.170	0.226
F_d (N)	0.082	0.395	0.968	1.678

Table 3. Drag forces at different incoming velocities in the laboratory experiments for attack angle of 90°.

u (m/s)	0.058	0.113	0.170	0.226
F_l (N)	0.032	0.131	0.321	0.534

Table 4. Lift forces at different incoming velocities in the laboratory experiments for attack angle of 45°.

When C_n is kept at a constant, the coefficient C_t increases with an increment of 2 from 6 to 12. As shown in Figure 13a, varying C_t has no effect on the flow field around the plane net for attack angle of 90°. However, when the plane net is positioned at a smaller attack angle; the flow velocity decreases with increasing C_t. As the attack angle decreases, the influence of variation of C_t to the flow velocity increases. When C_t is a constant, the flow velocity decreases linearly with increasing C_n (see Figure 13b). In addition, the variation tendencies are almost the same for different attack angles. With a same increment of 6, the coefficients C_t and C_n have different influence on the flow field around the plane net. The maximum discrepancies in flow velocity are 4.3% for the variation of C_t at an attack angle of 30° and 2.1% for the variation of C_n at an attack angle of 90° respectively.

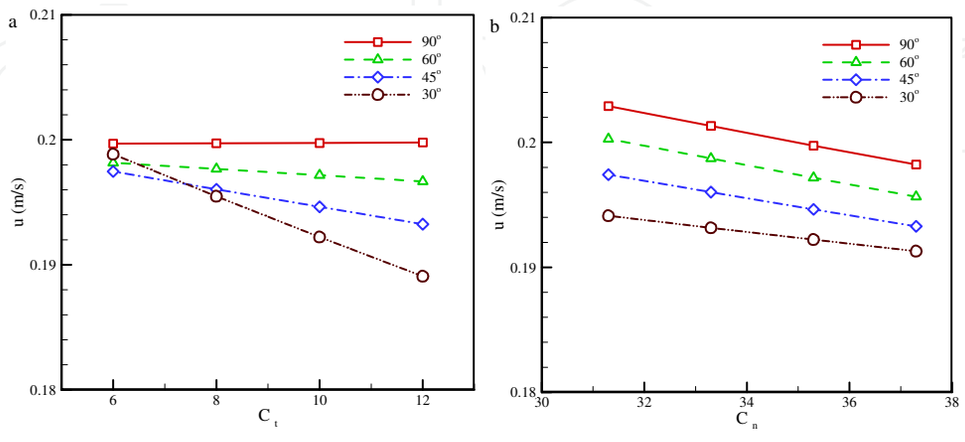

Figure 13. Comparisons of the flow velocity 0.6 m downstream from the center of the fishing net calculated with different sets of porous coefficients: (a) varying C_t for C_n=35.3 m^{-1} and (b) varying C_n for C_t=10.0 m^{-1}.

3.7. Brief conclusion

In summary, numerical results depends on the different model parameters to some extent. Appropriate values of the thickness of the porous media, the grid refinement and the time-step size are beneficial to reducing the computational effort and keeping high calculation accuracy. The mesh-grouping method can be used to reduce the number of plane-net elements and the computational effort. Two iterations are sufficient to achieve a converged solution of a flexible fishing net. The porous coefficients have a significant effect on the flow velocity around the fishing net and the relationship between each coefficient and the flow velocity is approximately linear. In addition, the influence of the coefficient C_t to the flow velocity is different with different attack angles. Based on the above, the initial values (see Table 1) are the optimal parameters for the numerical model.

4. The advantage of the coupled model

In present numerical model, the fluid-structure interaction (FSI) between flow and fishing net is taken into consideration. Because of the shielding effect of the fishing net, there exist the flow-velocity-reduction regions upstream of and downstream from the fishing net (see Figure 14). According to the numerical simulation, the reduction regions become smaller when considering FSI due to the decrease in height of the fishing net. However, the flow-velocity reduction is larger than that without considering FSI downstream from the fishing net. In the numerical results, the streamlines present the flow direction (see Figure 14). It was determined that the diversion of flow direction around the fishing net is relatively small but more obvious than that without considering FSI.

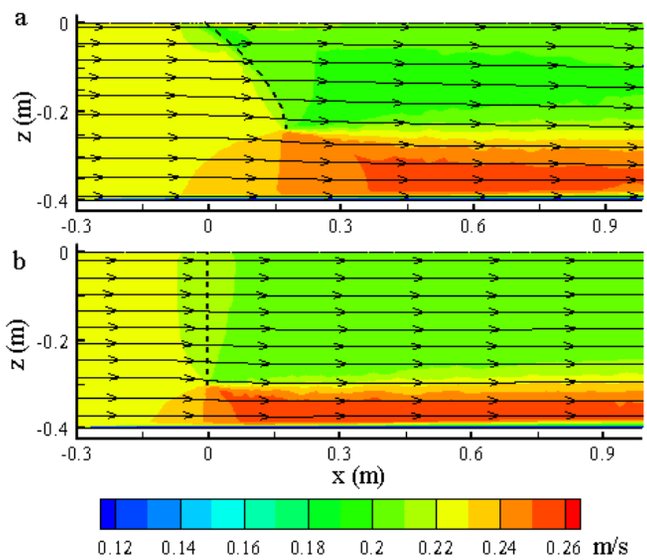

Figure 14. Flow-velocity distribution on the vertical plane y=0 around the net calculated by numerical simulation for incoming velocity of 0.226 m/s: (a) considering FSI between flow and fishing net and (b) without considering FSI.

Comparing the flow-velocity distribution along the *x*-direction, there exists rather obvious discrepancy between the fishing net with and without considering FSI (see Figure 15). The flow velocity upstream of the fishing net is greater than that without considering FSI, while the flow velocity downstream is smaller. The maximum flow-velocity reductions downstream are 15.0% for the FSI model and 11.9% for the model without considering FSI, respectively. It was found that the deformed net has more obvious shielding effect than the net with no deformation. This is due to the deformation of the flexible net. When exposed to current, the flexible net changes its shape and deviates from the original position. If the net is evenly divided into several plane-net elements, the angle between the incoming current and each net element (attack angle) decreases. Thus there is a relative increase in net solidity along the flow direction, and resulting in a more obvious blockage effect.

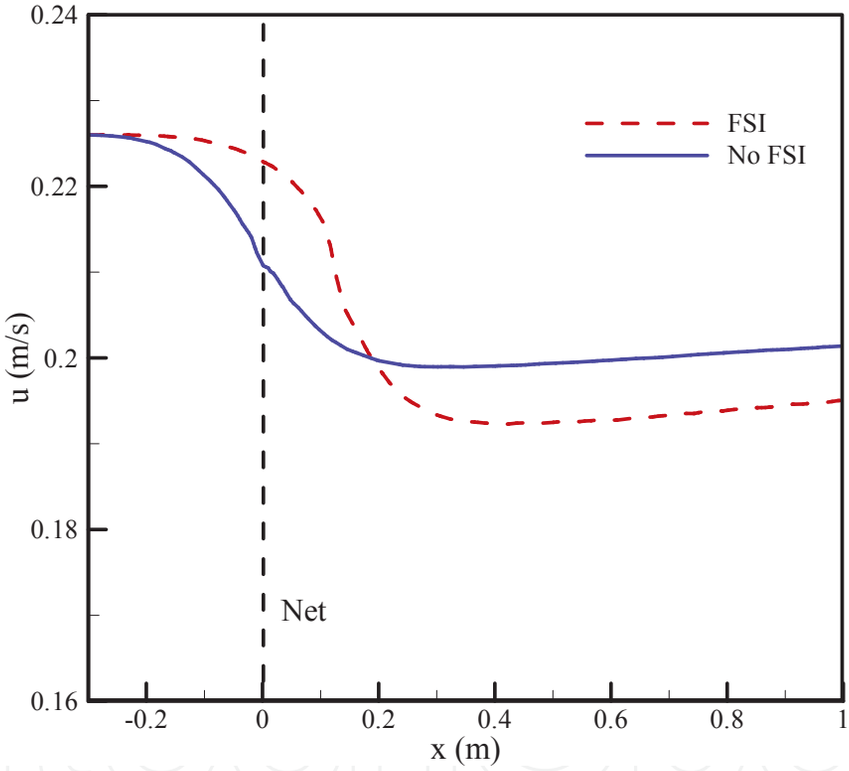

Figure 15. Comparisons of the flow-velocity component *u* along a line through the net in the *x*-direction with and without considering FSI for incoming velocity of 0.226 m/s. The straight line is *y*=0 on the horizontal plane *z*=–0.15 m.

As shown in Figure 16, the deformation of the fishing net is less serious than that without considering FSI. This is because that the net configuration is calculated based on the actual velocity acting on the flexible net instead of the incoming velocity in present numerical model. The actual velocity is slightly smaller than the incoming velocity due to the blockage effect of the net. As a result, the drag force is a bit smaller at approximately 7-8% than that without considering FSI for different incoming velocities (see Figure 17).

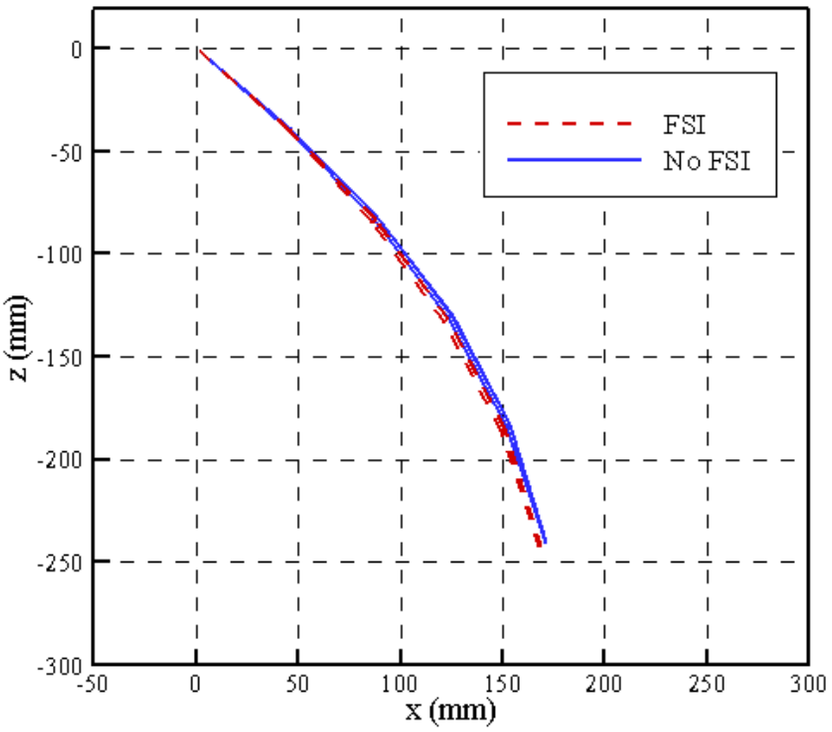

Figure 16. Comparison of the net configurations with and without considering FSI for incoming velocity of 0.226 m/s.

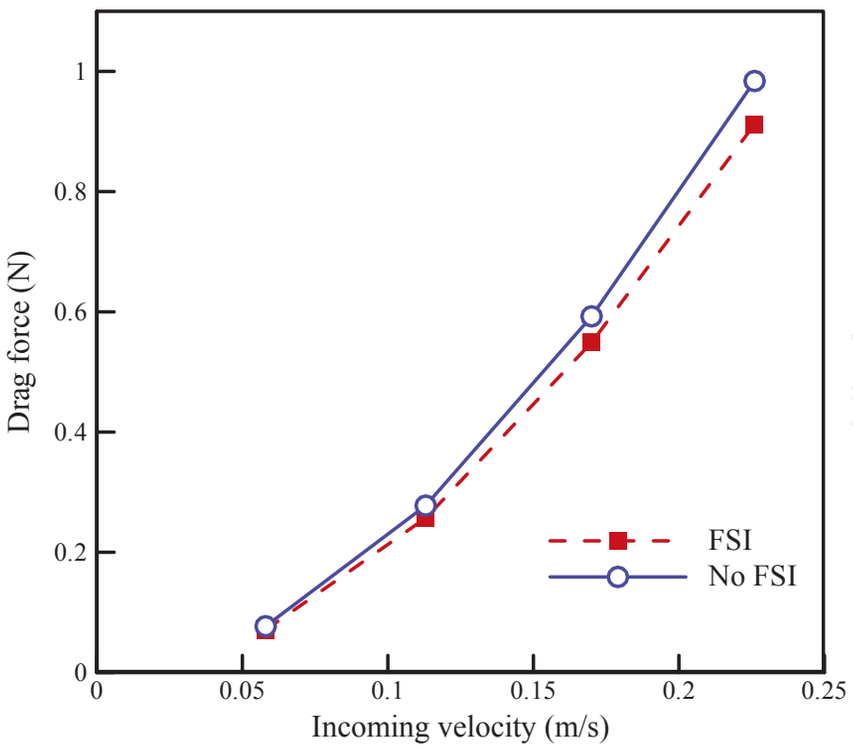

Figure 17. Comparisons of the drag force with and without considering FSI at different current velocities.

According to the analyses above, there are obvious difference between the flow field, the hydrodynamic force and the deformation of the fishing net with and without considering FSI. For multiple nets, the influence of FSI on the hydrodynamic characteristics of the fishing net will become more obvious. Therefore, it is necessary to take FSI into consideration in studying the interaction between flow and fishing net.

5. Conclusions

A numerical model is proposed to simulate the interaction between flow and fishing net based on the joint use of the porous-media fluid model and the lumped-mass mechanical model. Convergence studies are performed to analyze the influence of different model parameters on the numerical results and a set of optimal parameters are obtained for the numerical model. The numerical results of net deformation, drag force and flow velocity around the fishing net agree well with the experimental data. It is indicated that present numerical model can simulate the interaction between flow and fishing net accurately.

Compared with the numerical results without considering FSI, present numerical model is considered to present more accurate results: (i) the flow-velocity reduction is larger downstream from the fishing net, (ii) the diversion of flow direction around the fishing net is more obvious, (iii) the deformation of the fishing net is less serious and (iv) the drag force is a bit smaller at approximately 7-8% for different incoming velocities.

This study forms a foundation for studying the flow field and hydrodynamic characteristics of net cages and offers some valuable information for the aquaculture industry.

Acknowledgements

This work was financially supported by the National Natural Science Foundation (NSFC) Project Nos. 51239002, 51221961 and 51109022 and the Fundamental Research Funds for the Central Universities (DUT13LK55).

Author details

Chunwei Bi, Yunpeng Zhao* and Guohai Dong

*Address all correspondence to: Zhaoyp18@hotmail.com

State Key Laboratory of Coastal and Offshore Engineering, Dalian University of Technology, Dalian, China

References

[1] Aarsnes JV, Rudi H, Løland G. Current forces on cage, net deflection. In: Engineering for Offshore Fish Farming, Oct 17-18, Thomas Telford, London, 1990. pp. 137–152.

[2] Lader PF, Enerhaug B. Experimental investigation of forces and geometry of a net cage in uniform flow. IEEE Journal of Oceanic Engineering 2005; 30 (1): 79–84.

[3] Fredriksson DW, DeCew JC, Tsukrov I, Swift MR, Irish JD. Development of large fish farm numerical modeling techniques with in situ mooring tension comparisons. Aquacultural Engineering 2007; 36 (2): 137–148.

[4] DeCew J, Tsukrov I, Risso A, Swift MR, Celikkol B. Modeling of dynamic behavior of a single-point moored submersible fish cage under currents. Aquacultural Engineering 2010; 43 (2): 38–45.

[5] Huang CC, Tang HJ, Pan JY. Numerical modeling of a single-point mooring cage with a frontal rigid frame. IEEE Journal of Oceanic Engineering 2009; 34 (2): 113–122.

[6] Xu TJ, Zhao YP, Dong GH, Li YC, Gui FK. Analysis of hydrodynamic behaviors of multiple net cages in combined wave-current flow. Journal of Fluids and Structures 2013; 39: 222–236.

[7] Zhao YP, Bi CW, Dong GH, Gui FK, Cui Y, Guan CT, Xu TJ. Numerical simulation of the flow around fishing plane nets using the porous-media model. Ocean Engineering 2013; 62: 25–37.

[8] Zhao YP, Bi CW, Dong GH, Gui FK, Cui Y, Xu TJ. Numerical simulation of the flow field inside and around gravity cages. Aquacultural Engineering 2013; 52: 1–13.

[9] Bi CW, Zhao YP, Dong GH, Xu TJ, Gui FK. Numerical simulation of the interaction between flow and flexible nets. Journal of Fluids and Structures 2014; 45:180–201.

[10] Bi CW, Zhao YP, Dong GH, Zheng YN, Gui FK. A numerical analysis on the hydrodynamic characteristics of net cages using coupled fluid–structure interaction model. Aquacultural Engineering 2014; 19: 1–12.

[11] Burcharth HF, Andersen OH. On the one-dimensional steady and unsteady porous flow equations. Coastal Engineering 1995; 24 (3–4): 233–257.

[12] Balash C, Colbourne B, Bose N, Raman-Nair W. Aquaculture net drag force and added mass. Aquacultural Engineering 2009; 41 (1): 14–21.

[13] Tsukrov I, Drach A, DeCew J, Swift MR, Celikkol B. Characterization of geometry and normal drag coefficients of copper nets. Ocean Engineering 2011; 38 (17-18): 1979–1988.

[14] Zhan JM, Jia XP, Li YS, Sun MG, Guo GX, Hu YZ. Analytical and experimental investigation of drag on nets of fish cages, Aquacultural Engineering 2006; 35 (1): 91–101.

[15] Bear J. Dynamics of fluids in porous media. America Elsevier Publishing Company, Inc., New York, USA, 1972.

[16] Li YC, Zhao YP, Gui FK, Teng B. Numerical simulation of the hydrodynamic behaviour of submerged plane nets in current. Ocean Engineering 2006; 33(17-18): 2352–2368.

[17] Zhao YP, Li YC, Gui FK, Dong GH. Numerical simulation of the effects of weight system on the hydrodynamic behavior of 3-D net of gravity cage in current. Journal of Hydrodynamics, Series B 2007; 19 (4): 442–452.

[18] Tsukrov I, Eroshkin O, Fredriksson DW, Swift MR, Celikkol B. Finite element modeling of net panels using a consistent net element. Ocean Engineering 2003; 30 (2): 251–270.

[19] Zhao YP, Li YC, Dong GH, Gui FK, Teng B. Numerical simulation of the effects of structure size ratio and mesh type on three-dimensional deformation of the fishing-net gravity cage in current. Aquacultural Engineering 2007; 36 (3): 285–301.

IntechOpen